CHAPTER

Photoelectrocatalytic Reduction of Carbon Dioxide

12

Yong Yan, Jing Gu, Elizabeth L. Zeitler, Andrew B. Bocarsly
Department of Chemistry, Princeton University, Princeton, NJ, US

CHAPTER OUTLINE

12.1 Introduction

Research on the reduction of carbon dioxide (CO_2) is strongly motivated by concerns about the steadily increasing accumulation of carbon dioxide in the atmosphere, from a concentration of 270 ppm before the industrial revolution to 400 ppm (and rising) today.[1] A feasible route to recycle and utilize environmentally deleterious CO_2 emissions requires two chemical processes: (1) Capture of carbon dioxide from major point sources as well as directly from the atmosphere[2,3] (2) Conversion of the captured carbon dioxide into value added organics[4] of use as industrial feedstock[5] or fuels.[4,6,7] The importance of carbon dioxide reduction not only lies in concerns about global warming, but also has implications for solar energy storage via carbonaceous liquid fuels.[2] Combining renewable energy storage with CO_2 reduction to small organics/fuels/industrial feedstocks is not new, but, progress in this area has been limited due to the challenges presented by the thermodynamic and kinetic stability of CO_2. This is especially pertinent when comparing

Carbon Dioxide Utilisation. http://dx.doi.org/10.1016/B978-0-444-62746-9.00012-8

one-electron reduction of CO_2 to multielectron/multiproton processes. Thus, catalyst development is central to progress in both the photochemical and electrochemical transformation of CO_2 to desirable organic products.[8]

'Catalysis' as a term has been imprecisely applied in electrochemistry and photoelectrochemistry, leading to some confusion related to photoelectrocatalysts in particular. By definition, catalysis to form a chosen product requires a thermodynamically favourable reaction ($\Delta G^0 < 0$) since the role of a catalyst is only to lower the kinetic barrier to the reaction ($\Delta G^{\ddagger}$), not to provide the energy input needed to push an equilibrium toward desired products. The standard redox potential (E_R^o) is related to the electrochemical energy required to overcome a positive free energy of reaction as shown in Eqn (12.1):

$$\Delta G^0 = -nFE_R^o \tag{12.1}$$

If one considers electrons as one of the 'reactants' in a redox reaction, then an applied electrode potential adjusts the reactant energy to drive the reaction, and such externally added energy is not considered catalytic. In general, the applied potential will need to be greater than the standard potential to accommodate the free energy needed to overcome the activation barrier, $\Delta G^{\ddagger}$. The difference between the Nernstian potential, E_R, and the operating potential of the system is referred to as the overpotential, and is the potential beyond the redox potential required to obtain a given current for a reaction. An electrocatalyst minimizes the overall applied potential by lowering the overpotential. Thus, by definition an electrocatalyst must reduce the overpotential of a reaction, but cannot reduce the overpotential below zero (i.e., generate an underpotential) since doing so would imply that the catalyst was changing the ground state thermodynamics of the system (that is shifting the value of ΔG^0).

As an alternative to the direct application of an electrode potential, redox reactions can also be driven by absorption of light energy into a semiconducting electrode. Such a system is referred to as a photoelectrochemical cell (PEC) and involves the generation of a photopotential at the semiconductor–electrolyte interface. In contrast to an applied electrochemical potential, which is not considered catalytic, the use of light energy to promote electrons and drive otherwise unfavourable reactions is often described as 'photocatalysis'. Photocatalysis used thus is not catalysis because it describes providing light energy to overcome a positive ($\Delta G + \Delta G^{\ddagger}$) of reaction, rather than lowering the kinetic barrier to reaction. However, the term photocatalytic is widely accepted and understood to refer to a process that is accelerated by adsorption of light energy to compensate for a positive ΔG of reaction. Within the context developed here, one can then speak of reactions occurring at an 'underpotential' at a semiconductor electrode, which simply means that the electrode is photocatalytically coupling the incident light energy into both the ΔG and $\Delta G^{\ddagger}$ of reaction to produce a net negative reaction free energy relative to reductions available at an ideally reversible electrode. The PEC system may also be electrocatalytic in that the electrode surface or other components of the system may serve to lower the intrinsic reaction barrier ($\Delta G^{\ddagger}$). Thus, the reduction in operating potential in a photoelectrochemical system when compared to the same reaction occurring at a

metal electrode is a combined effect of the light energy driving the reaction thermodynamics and the charge transfer kinetics.

Because solar energy can drive photoelectrochemical reactions, the application of solar irradiation in reduction processes provides a direct route towards storing solar energy as chemical bonds, or so called solar fuels. The terms 'artificial photosynthesis' and 'reverse combustion' have been applied to suggest the sense of the reaction strategy for light-driven CO_2 reduction, especially to fuels and other energy storage products. Hydrogen is the simplest fuel molecule, but it has limitations due to being a gas at standard temperature and pressure (STP). Storing solar energy as liquid organics, i.e., methanol, ethanol etc. are more interesting targets for artificial photosynthesis as these materials are easier to handle and more applicable to direct use. The primary stumbling block to solar energy conversion into carbon containing fuels is the chemical stability of CO_2, which leads to significantly less favourable kinetics for fuel formation relative to H_2 reduction from water. Direct one-electron reduction of CO_2 is reported to require ~ -2.1 V vs SCE[4] (all potentials in this chapter are versus a saturated calomel electrode/half cell (SCE), unless otherwise noted), however, very little of this energy is stored in its reduced product as indicated by the potentials given in Scheme 12.1. For instance, 690 kJ/mol of free energy is stored upon the formation of methanol and oxygen from CO_2 and H_2O under standard conditions, but if this process needs to be carried out at -2.1 V (and assuming 400 mV of overpotential for oxygen formation) 1.7×10^3 kJ/mol needs to be expended. Without a catalyst that can bypass the direct one-electron reduction of CO_2 this process results in a great amount of applied electrical or incident light energy wasted.

Early research on 'reverse combustion' dates back 150 years, in which aqueous carbon dioxide or bicarbonate was reduced to form formic acid.[9] Hori et al. accelerated this research field during 1960s by screening most elemental metals as electrodes to determine aqueous CO_2 electrochemical reduction products and their relative overpotentials.[10] The field attracted significant attention a decade later, when photoelectrochemistry sparked interest in utilizing solar energy for CO_2 conversion. Hydrogen production from water was initially examined for solar fuels, and thereafter was extended to carbon fuels from CO_2 reduction. Such research directions were spurred by the energy crisis in 1970s when petroleum costs in the United

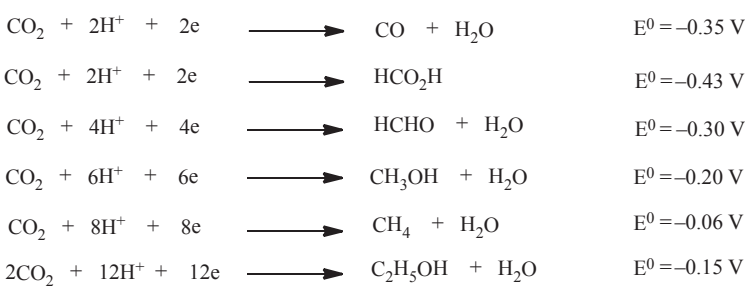

SCHEME 12.1

Carbon dioxide reduction potentials vs SCE under standard conditions (pH = 0).

States were dramatically increased. Recently, advanced research into CO_2 photoelectrochemical reduction has been reactivated since both environmental and renewable energy concerns again are attracting scientific and public attentions. These new pursuits are further enabled by the development of modern photochemistry, electrochemistry and material science, particularly the materials chemistry of inorganic semiconductors. Current research focuses on enhancing incident light energy usage efficiency, especially solar energy capture efficiency and CO_2 conversion kinetics for photoelectrocatalytic CO_2 reduction.

In this chapter, semiconductor photocatalyst/electrode and light-activated molecular homogeneous catalysts for CO_2 reduction will be examined from earlier work as well as very recent findings. The review begins with a discussion of the relevant parameters for photodriven CO_2 reduction. Having defined the problem, discussion of the literature is provided and organized by the mechanistic approaches to light-fuelled CO_2 reduction, including photovoltaic/electrolyser combined systems, semiconductor nanomaterials in photochemical systems, photoelectrodes modified with homogeneous or coordinatively attached molecular catalysts or photoelectrode surfaces modified by metal co-catalysts. Current research has exposed a number of new avenues to explore, which may provide one or more pathways to industrial scale CO_2 reduction to fuels. But, in this regard, this research field is still in its formative stages.

12.2 Organizing principles of photoelectrochemical CO_2 reduction

Efficiency of CO_2 reduction or any photochemical process is expressed as quantum yield: the percent of light energy input converted to chemical energy output. Quantum yield (Φ) is the fundamental energy metric for photochemistry and photoelectrochemistry. In homogeneous systems for CO_2 reduction, quantum yield can be easily determined by moles of products versus moles of absorbed photons, while catalytic turnover numbers can be determined by moles of products per mole of catalyst. Determining the quantum yield and turnover number of semiconductor heterogeneous systems, however, is more complicated due to a lack of knowledge about the number of effective active sites for reduction catalysis. The quantum efficiency of the heterogeneous photocatalytic process is defined as the number of reduction events per photon incident (not absorbed).

A semiconductor's electronic structure possesses a void energy region where no states are available to promote recombination of an electron and hole produced by photo activation in the solid. This void region is called the band gap and extends from the highest energy level of the electron-occupied valence band to the lowest energy level of the vacant conduction band. As illustrated in Figure 12.1, upon photoexcitation with absorbed photon energy equal to or higher than the band gap, an electron from the valance band is promoted to the conduction band, leaving an empty state, called a hole, in the valance band. Following excitation, the generally nanosecond

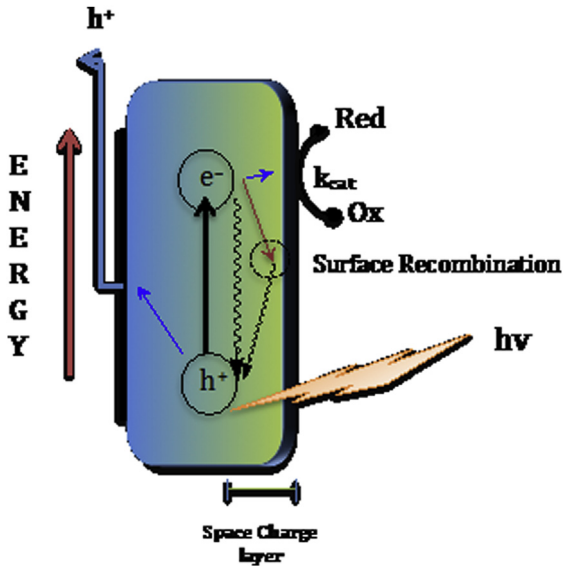

FIGURE 12.1 Typical electron–hole pair photophysical dynamics for an illuminated p-type semiconductor:

charge separation occurs upon photoexcitation with light energy greater than or equal to the band gap and is indicated by the solid black arrow. Recombination of carriers, parameterized by the rate constant k_R, occurs either in the bulk (wavy arrow) or at the semiconductor surface (solid arrow plus wavy arrow). The space charge region contains an electric field that spatially separates electrons and holes. For a p-type semiconductor, electrons are driven toward the electrolyte interface (blue—productive, and red—recombination arrows) and holes migrate toward the back of the semiconductor and into the external circuit via a backside ohmic contact (blue arrow). The interfacial charge separating electric field is depicted as band bending, which is illustrated later in this chapter (see Figure 12.3 Once electrons arrive at the semiconductor–electrolyte interface, a separate process(es) (k_{cat}) moves the charge from the semiconductor to the solution species. If k_{cat} is small then surface recombination can dominate the overall chemistry. The hole transfers through the external circuit to the anode where an oxidation process takes place.

long-lived electron–hole pair[11] can effect charge transfer to either the adsorbed co-catalyst or CO_2 itself. However, in the absence of a barrier, charge recombination is inevitable and can seriously decrease the quantum yield of CO_2 reduction.

However, as illustrated in Figure 12.1 and 12.3 the excited state lifetime of the electron–hole pairs generated under illumination (and in the vicinity of the semiconductor surface) can be prolonged by establishing an electric field at the semiconductor–electrolyte interface. This field induces a spatial separation of the photogenerated electron and hole, causing one of these species (depending on the field vector) to migrate to the surface of the photoelectrode. In the case, of a p-type semiconductor the interfacial field drives electrons toward the electrode

surface. Efficient promotion of the surface charge carrier through the interface and onto a CO_2 reactant is required, since even in the presence of an interfacial electric field surface charge recombination is relatively facile. Additionally, even before charge carriers arrive at the semiconductor–electrolyte interface some degree of charge recombination in the volume of the semiconductor can occur. Thus, to determine the CO_2 reduction efficiency or quantum yield of a semiconductor system, a combination of all the pathway probabilities for the electron and hole must be considered. Thereby, the quantum yield can be defined by rate of the charge transfer and recombination processes as shown in Eqn. (12.2):

$$\Phi = k_C/(k_C + k_R) \tag{12.2}$$

Where k_C is the rate constant for interfacial charge transfer and k_R is a rate constant summarizing all of the electron–hole recombination pathways outlined in Figure 12.1. Upon interfacial charge transfer reactivity is solely dependent on the catalytic nature of the system. In short, the primary role of the semiconductor in photocatalysis is to absorb an incident photon, generate an electron–hole pair and facilitate its separation and transport, whereas catalysis of the reaction is an additional function, which is often performed either by the semiconductor surface or a different material.

In addition to defining the band gap, the conduction and valence band edges of the semiconductor also dictate the energetics of possible charge transfer reactions. Understanding of CO_2 reduction energetics relative to semiconductor band positions parameterizes the CO_2 reduction process. Figure 12.2 illustrates the conduction

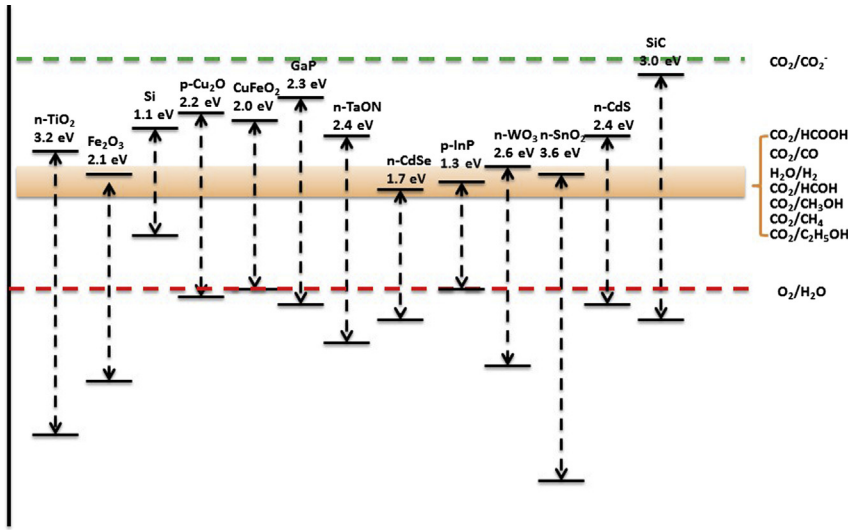

FIGURE 12.2 Conduction band and valance band relative potentials and band energies of common semiconductors.

Their relative band positions were compared with CO_2 reduction and water reduction and oxidation at pH = 0.

Data were extracted from References 2,12–15.

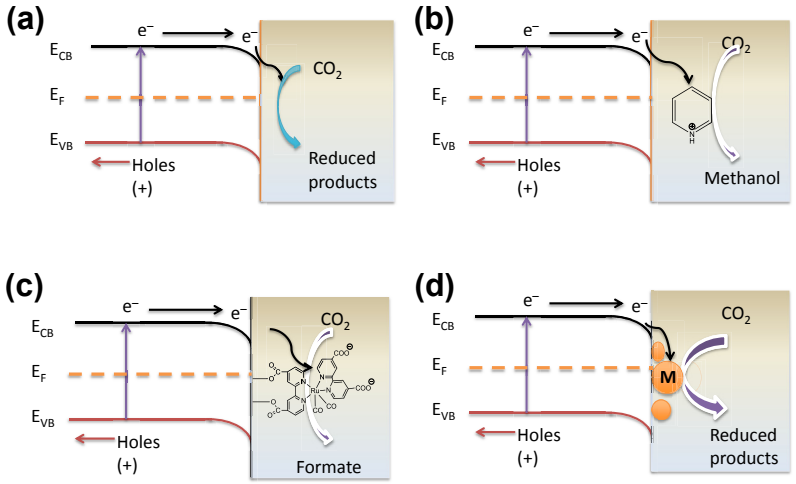

FIGURE 12.3 Illustrative band bending diagrams for p-type semiconductor photoelectrode photocatalytic reduction of CO_2:

(a) semiconductor material itself as CO_2 reduction catalyst; (b) homogeneous unattached catalyst (pyridinium for example); (c) molecular catalyst $[Ru(bpy)_2(CO)_2]$ attached on photoelectrode surface; (d) electrodeposited or nanoparticle casted metallic catalyst on the surface of semiconductor materials for CO_2 reduction. For further explanation refer to Figure 12.1.

and valence band position of common photoelectrodes that are reported to reduce CO_2. These band positions are compared with CO_2 reduction potentials to various products under standard conditions ($[H^+] = 1$ M). Note that under the standard conditions, many semiconductor materials become unstable, for example, p-Cu_2O reacts with acid resulting in complete copper dissolution. Figure 12.2 simply provides a theoretical comparison of the thermodynamic band energies; it does not indicate the optimal CO_2 reduction reactions.

In theory, as indicated in Figure 12.2, with the exception of the redox potential of the CO_2/CO_2^- redox couple residing higher than all the conduction band edges, the reduction potentials of CO_2 to common products lie well within the band gap of the majority of the semiconductors mentioned here. That is, the conduction band energies are in general higher than CO_2 reduction potentials, implying thermodynamically allowed electron transfers. Significantly, redox potentials of CO_2 reduction are limited to a very small range (from -0.06 V to -0.43 V vs SCE at $[H^+] = 1$ M). This potential range is indicated by the horizontal band in Figure 12.2. Note that this redox potential box will shift to more negative potential at a rate of -59 mV for every pH unit increase. As already noted, thermodynamically allowed processes do not imply that reductions will occur at an appreciable rate, multiple proton and multiple electron transfers need also be kinetically facile in these systems.

Unfortunately, unlike the thermodynamic potential comparisons, the theoretical understanding of semiconductor materials' catalytic principles towards CO_2 reduction is not well established. The formation of different reduced products from CO_2 heavily depended on the specific reaction pathways taken as well as the

couplings that occur between proton and electron transfers. Two-electron reduced products of CO, formic acid and oxalic acid; 4-electron product formaldehyde; 6-electron product methanol; and more than 6-electron products of methane, ethane, ethene, acetaldehyde, ethanol, higher carbon alcohols, higher carbon aldehydes and hydrocarbons have all been detected and reported as products of CO_2 reduction.[2,8,16,17] Current research is still highly results-driven: the capability to predict the catalytic ability of a specific semiconductor material or theoretically optimize a semiconductor system is not available.

12.3 Photovoltaic/electrolyser duel module systems: Metal electrodes for CO_2 conversion

Solar driven reduction of CO_2 has been achieved by combination of a commercial solar panel with a CO_2 electrolyser using electrocatalytic metal electrodes. The essential concept and the core chemistry rely on the direct electrochemical reduction of CO_2; however, the required electricity is generated by solar panels. Two companies that have recently announced development of such systems are Liquid Light Inc. and Det Norske Veritas. Both companies have combined classic electrolyser technology with commercial photovoltaic panels to carry out the CO_2 to formate conversion with a solar-to-combustion energy conversion efficiency approaching 2%. However, besides the engineering development of the electrochemical cell, the key chemistry is still reliant on the progress of electrocatalytic metal electrodes. To this end, prior work on metal electrodes, dating back to the early 1970s has been reinvestigated with a focus to improve electrode stability and catalysis via understanding and manipulating interfacial morphology and chemical composition. The present efforts in this area are based on Hori's pioneering work which is summarized in Table 12.1.[10]

Since Hori's original studies, the number of electrode materials investigated as cathodes for CO_2 reduction has continued to expand as summarized in Table 12.2. Recently, Kanan reported that copper[22] and gold[30] electrodes having unique nanoscale morphology were quite stable and efficiently reduced CO_2 to carbon monoxide, formate, methanol and other higher carbon products with significant higher yield than standard polycrystalline electrodes. An electrodeposited copper(I) oxide thin film surface was also reported by Flake et al. to selectively reduce CO_2 to methanol at 38% Faradaic yield.[21] Moreover, more than 16 chemical identifications within a wide range of C_1-C_3 products have been successfully achieved in a copper foil flow cell by Jaramillo.[16] The potential-dependence and current efficiency of each product was carefully compared in this work. The distinctive electrocatalytic ability of Cu towards CO_2 reduction inspired mechanistic investigations on this electrode. Asthagiri et al.[31] claimed the reduction of CO is the key selectivity-determining step for CO_2 electro-reduction on Cu(III). The dominant path proceeds through reduction of CO to COH, which eventually leads to CH_x species, and can produce both methane and ethylene. Although copper metal electrodes generate hydrocarbons during the electrochemical reduction of CO_2, the activity of these electrodes typically decreases after

Table 12.1 Faradaic Efficiencies of CO_2 Reduction Products at Common Metal Electrodes at 0.1 M $KHCO_3$

Electrode	Potential vs SHE V	Current Density mA/cm^2	Faradaic Efficiency %							
			CH_4	C_2H_4	EtOH[a]	PrOH[b]	CO	$HCOO^-$	H_2	Total
Pb	−1.63	5.0	0.0	0.0	0.0	0.0	0.0	97.4	5.0	102.4
Hg	−1.51	0.5	0.0	0.0	0.0	0.0	0.0	99.5	0.0	99.5
Tl	−1.60	5.0	0.0	0.0	0.0	0.0	0.0	95.1	6.2	101.3
In	−1.55	5.0	0.0	0.0	0.0	0.0	2.1	94.9	3.3	100.3
Sn	−1.48	5.0	0.0	0.0	0.0	0.0	7.1	88.4	4.6	100.1
Cd	−1.63	5.0	1.3	0.0	0.0	0.0	13.9	78.4	9.4	103.0
Bi[c]	−1.56	1.2	–	–	–	–	–	77	–	–
Au	−1.14	5.0	0.0	0.0	0.0	0.0	87.1	0.7	10.2	98.0
Ag	−1.37	5.0	0.0	0.0	0.0	0.0	81.5	0.8	12.4	94.6
Zn	−1.54	5.0	0.0	0.0	0.0	0.0	79.4	6.1	9.9	95.4
Pd	−1.20	5.0	2.9	0.0	0.0	0.0	28.3	2.8	26.2	60.2
Ga	−1.24	5.0	0.0	0.0	0.0	0.0	23.2	0.0	79.0	102.0
Cu	−1.44	5.0	33.3	25.5	5.7	3.0	1.3	9.4	20.5	103.5[d]
Ni	−1.48	5.0	1.8	0.1	0.0	0.0	0.0	1.4	88.9	92.4[e]
Fe	−0.91	5.0	0.0	0.0	0.0	0.0	0.0	0.0	94.8	94.8
Pt	−1.07	5.0	0.0	0.0	0.0	0.0	0.0	0.1	95.7	95.8
Ti	−1.60	5.0	0.0	0.0	0.0	0.0	Tr.	0.0	99.7	99.7

[a] *Ethanol.*
[b] n-*propanol.*
[c] *The data are taken from Hori et al.*[10] *except Bi which is read from an illustration in a paper by Komatsu et al.*[87].
[d] *The total value contains* C_2H_5OH*(1.4%),* CH_3CHO*(1.1%),* C_2H_5CHO*(2.3%) in addition to the tabulated substances.*
[e] *The total value contains* C_2H_6*(0.2%).*
Permission from Elsevier Reference 10.

Table 12.2 Recent Developments in Electrocatalytic CO_2 Reduction at Various Metal Electrodes Using Surface Morphology Control or a Soluble Co-Catalyst

Metal Electrode	Ref.	Potential (V, vs)[a]	Electrolyte	Current Density	Products (Faradaic Yield[f])
Cu on diamond	19	−1.3 NHE	IL with H_2O	5.1 mA^2/cm	Formic acid, formaldehyde, $C_xH_yO_z$
Cu/Au alloys	20	−0.65 RHE	0.5 M $KHCO_3$	1 mA^2/cm^2	Products not specified
Cu (ox-layer)	21	−1.1 SCE	0.5 M $KHCO_3$	43[e]	Methanol (38%)
Cu (flow cell)	16	PD[b]	0.1 M $KHCO_3$	PD	PD: 16 products
Cu (ox-derived)	22	−0.5 RHE	0.5 M $NaHCO_3$	3 mA^2/cm^2	PD; formate (40%); CO, methane, ethane
Ag in IL	23	1.5[c]	IL with H_2O	10 mA^2/cm	CO (95%); H_2 (5%)
Pt (pyridinium)	24,25	−0.6 SCE	0.5 M KCl	1 mA^2/cm	Methanol (22%), formic acid (10.8%)
Bi in IL	26	−1.95 SCE	IL/MeCN	–	CO (99%), H_2 (less than 1%)
Sn (oxo-derived)	27	−0.7 RHE	0.5 M $NaHCO_3$	4 mA^2/cm^2	PD; formic acid (19%); CO,
In (solar)	28	Zero bias[d]	0.5 M $KHCO_3$	–	Formic acid (28% quantum yield max)
In in IL	29	−1.4 AgCl/Ag	3 M NaCl	4 mA^2/cm^2	Formate (80–100%)
Au (ox-derived)	30	−0.25 RHE	0.5 M $NaHCO_3$	0.8 mA^2/cm	PD; CO (80%)

[a] *Potentials directly derived from electrolysis data of reference.*
[b] *PD: potential dependence.*
[c] *Two-electrode setup, vs Pt anode.*
[d] *Solar energy via PV only, no other potential applied.*
[e] *Methanol yield density: 43 $\mu mol/cm^2/h$.*
[f] *Faradaic yield unless other specified.*

several minutes of operation.[32] To overcome this problem a pulse electrolysis mode with anodic as well as cathodic polarization was applied to the copper electrode. CH_4 and C_2H_4 hydrocarbon species were found to be the main products, and the activity of the electrode was maintained for at least 1 h. The enhanced stability was associated with a proposed copper oxide species formed on the Cu electrode surface. The selectivity of C_2H_4 species over CH_4 species was further improved when electrochemical reduction was applied directly on copper oxide electrode; the highest efficiency of about 28% was obtained at −3.15 V vs Ag/AgCl.

The Norskov group[18,33] has systematically studied the binding kinetics of CO_2 and its reductive intermediates on copper surfaces and demonstrated that the relative kinetic barriers to C−C coupling decrease significantly with the degree of hydrogenation of reacting adsorbates. They have explained how copper can catalyse the production of higher hydrocarbons and oxygenates in the electrochemical environment, despite producing only single carbon atom products in gas-phase catalysis, and how C−C bonds can be formed in the room temperature electrochemical environment, whereas substantially higher temperatures were needed in Fischer−Tropsch catalysis.

Thanks to the rapid development of nanotechnology, similar studies of CO_2 electrochemistry have been reported for metal materials with or derived from nanostructured precursors. For instance, Kanan's group also studied quite similar oxide formation methodology on other metals: including Sn[27] and Au[30]. Higher selectivity and yield of CO_2 reduction products have been attributed to oxide layers formed on these metal electrode surfaces. A nanoparticulate form of copper decorated on a diamond electrode[19] exhibited atypical CO_2 reduction activity: not only the common reduced products CO, H_2, formate but also highly reduced methane, ethane, methanol, ethanol and isopropanol were detected in measurable yield. Bismuth metal electrodes showed interesting high current density in an asymmetric imidazolium ionic liquid in terms of CO formation.[26] A silver electrode in similar aqueous/ionic liquid electrolyte was also reported by Masel et al. to reduce CO_2 to CO and oxidized water to oxygen in a two-electrode system with total overpotential less than 200 mV.[23] Other electrodes such as indium,[28] platinum under pyridinium catalyst[24,25] and CuAu[20] alloys, in small particles or other morphologies at electrode surface structures are summarized at Table 12.2.

12.3.1 Semiconductor electrodes for CO_2 reduction

Heterogeneous photoelectrocatalytic reduction of CO_2 on semiconductor interfaces has been extensively investigated since the 1980s. This area of study was initiated by Halmann's report that one could photoelectrochemically reduce CO_2 to methanol with 60% Faradaic yield, using a p-type GaP photocathode in a liquid junction cell.[34] We discuss here some of the well-studied semiconductor electrode materials (group III−V: GaP, InP, GaAs; Group II−VI: CdS, CdSe; oxide Photoelectrodes: Cu_2O, $CuFeO_2$, TiO_2, TaON, WO_3, etc.) for direct CO_2 reduction in the next section and offer insight into possible mechanistic paradigms.

Although the mechanisms of catalysis for the direct reduction of CO_2 on photoelectrodes is not well understood, this area of research is quite active and typically involves mediation by coordinatively attached or uncoordinatively dispersed molecular catalysts and deposited nanoparticulate metal catalysts on the semiconductor interface. Four types of semiconductor/liquid junctions have been shown to photoassist CO_2 reduction as outlined in Figure 12.3. Direct CO_2 reduction at semiconductor electrodes (a) for example, light-activated GaP catalysed CO_2 to methanol conversion.[34] Dispersed molecular catalyst assisted CO_2 reduction (b) exemplified by aqueous pyridinium at a p-GaP(111) interface leading to selective CO_2 to methanol reduction at almost 100% Faradaic yield.[6] Coordinated/attached molecular catalyst assisted CO_2 reduction (c) homogeneous catalyst $[Ru(bpy)_2(CO)_{2s}]$ chemically attached to a Ta_2O_5 and InP semiconductor surface.[35,36] (d) Finally, metal particle decorated photoelectrodes for CO_2 reduction.[37]

12.4 Group III–V: GaP, InP, GaAs as photocathode for CO_2 reduction

GaP, which has an indirect band gap of 2.3 eV and a direct band gap of 2.8 eV, has been thoroughly investigated as a photoelectrode for CO_2 conversion. As already noted, Halmann's report using a p-type GaP photocathode was one of the earliest studies on the photoelectrochemical reduction of aqueous carbon dioxide, producing optical conversion efficiencies at 365 nm of 3–5%.[38] Based on this concept, one year later, Inoue et al. investigated photocatalytic reduction of carbon dioxide in aqueous suspensions of semiconductor powders.[39] Up to 10^{-3} M of formic acid, formaldehyde, methanol and methane were found as products and the role of the semiconductor suspensions was claimed to be both photosensitizer and catalyst. Under high pressure conditions, maximum Faradaic yield of 80% could be obtained with a cathodic bias of −1.0 V (vs SCE), in 0.5 M Na_2CO_3 and 8.5 atm pressure of CO_2.[40] The Faradaic yield was reported to decrease if the reaction was carried out at more negative potentials. This phenomenon was explained by the fact that GaP is more stable towards anodic decomposition at a less negative potential. Phase sensitive studies demonstrated that the photocathodic response of the p-GaP electrode was due to band gap excitation.[41] In pH = 7 buffered solution, the cathodic photocurrent increased about 15% when CO_2 was bubbled into the solution compared to Ar. Trace amounts of formate as product were detected at bias potentials of −1.54 V vs SCE. Recently, Bocarsly et al. found the combination of p-GaP electrode and pyridnium as catalyst increased the selectivity and efficiency of methanol production.[42] This will be further discussed in the section of semiconductor with a molecular co-catalyst.

The semiconductor electrode InP has a band gap of 1.34 eV, which is almost ideal for the efficient conversion of solar energy into electrical or chemical energy. The photoelectrochemical reduction of carbon dioxide at p-InP was studied in methanol,[43] in which CO_2 solubility is reported to be five times larger than found in aqueous solution at ambient conditions. The onset potential of the photocathodic current was −0.8 V. Compared to metallic electrodes, a positive onset potential shift

of 0.3−1.0 V by this electrode can be achieved by the photoassisted conversion process. The main product was identified as CO and maximum current efficiency was found at −2.5 V to be 41.5% and formic acid generation efficiency was found to be 15%.[43] Hirota et al. have investigated photoelectrolysis of CO_2 at p-InP under high pressure in a methanol medium.[44,45] The onset photopotential for CO_2 reduction initiated at −0.6 V, which is 0.4 V more positive compared with an Ar atmosphere. In a CO_2 saturated high pressure solution (40 atm.), CO was obtained with a current efficiency of 87−93% at constant current densities in the 50−100 mA/cm^2 range. Methyl formate formed by formate reacting with methanol was also identified as one of the products (Faradaic yield ranging from 3.5 % to 16%). At high CO_2 pressure light intensity was found to be the limiting factor.

P-GaAs electrodes, with a 1.42 eV band gap, have been extensively studied as photocathodes for solar to electrical energy conversion. Reduction of carbon dioxide on this electrode in the presence of various redox couples, which possibly act as electron relays in an aqueous solution, has been investigated by Zafrir et al.[46] To prevent the photocorrosion of the GaAs semiconductor surface, the vanadium redox couple V(III)/V(II) has been introduced, which provides more efficient electron transfer from the semiconductor surface to CO_2. With 0.32 M vanadium chloride in a 4 M HCl solution, at −0.5 V vs SCE, the current efficiencies for formate, formaldehyde and methanol were 0.04%, 0.017% and 0.012%, respectively. The major product in this process is hydrogen (from water). P-GaAs, similar to InP, has been also studied for CO_2 conversion under high-pressure in a methanol medium.[44,45] A current efficiency of 24.9% for CO production reached a maximum at −2.4 V. The Faradaic efficiency for the formation of methyl formate was in the range of 12−15% at potentials from −2.2 V to −2.5 V(vs Ag/AgCl).

GaN electrodes and the corresponding AlGaN/GaN photoelectrodes were studied by Yotsuhashi et al.[47,48] N-type GaN was used as photoanode and Cu metal as a counter cathode in an aqueous solution with a Nafion film used as a cation exchange membrane. Hydrogen, CO, CH_4, C_2H_4 and C_2H_6 were detected without any external energy source except light irradiation. Three percent Faradic efficiency was achieved for formate production in this system. In a modified device, the photoanode was separated into two parts: an electrically conducting layer containing n-type GaN and a photoabsorbing layer of unintentionally doped AlGaN. A NiO co-catalyst was also added to the device. These changes improved the conversion efficiency from 3 to 8.9%. A similarly engineered AlGaN/GaN system produced a 14% conversion efficiency. These reports suggest that new III−V semiconductors should be developed for the solar energy CO_2 conversion.

12.5 Group II−VI: CdTe, and Group IV: Si, SiC photoelectrodes

In addition to the Group III−V semiconductors, materials which combine group II and VI elements have been investigated for CO_2 reduction. Taniguchi et al. first noted the reduction of CO_2 to CO at a p-CdTe electrode, producing 70% Faradaic

efficiency at −1.6 V vs SCE in a DMF electrolyte with 1% water. They compared their system to an In metal electrode, and found that the photopotential on the semiconductor resulted in a 30% efficiency improvement over the metal system.[49] Soon after the initial reports of CO_2 reduction at p-CdTe, IR spectroscopy was used to detect intermediates at the electrode surface, and in acetonitrile four potential-dependent signals were observed which were attributed to formation of CO_2^- at the electrode surface.[50] Electrolyte variation was examined to elucidate the mechanism of CO_2 reduction at II−VI electrodes. Taniguchi found that yields were consistent for DMF, DMSO and propylene carbonate electrolytes and shifted towards less CO and more H_2 for acetonitrile. Supporting electrolytes with lithium and sodium deposited on the electrodes and caused decreased current for CO formation.[51] In aqueous electrolyte, p-CdTe was found to produce CO and formic acid at more modest potentials between −1 and −1.4 V vs SCE. The supporting electrolyte significantly affected the product distribution; more formic acid was produced in the presence of carbonate electrolytes and more CO was favoured in the presence of sulphates and phosphates, with markedly more CO formed in tetraethylammonium phosphate (TEAP) supporting electrolyte where H_2 production was also sharply curtailed.[52] The suppressed CO production in carbonate electrolytes was explained using the common ion effect because CO formation would also produce carbonate in an ECEC mechanism. Tetraalkylammonium ions were suggested to produce a hydrophobic environment at the electrode surfaces, favouring CO formation. Tetraalkylammonium ions however, may not be innocent in reduction of CO_2. In DMF it is suggested that this cation is a charge transfer mediator either in solution[53] or at the electrode surface.[54,55] A problem with p-type CdTe electrodes is their reported instability during CO_2 reduction in both aqueous[52] or nonaqueous electrolytes.[54]

Group IV semiconductors including silicon and silicon carbide are reported to photoelectrochemically reduce carbon dioxide. For example, illuminated p-Si electrodes were found to produce CO at −2 V, more negative potentials than observed for p-CdTe or p-GaP,[51] A powder of silicon carbide suspended in water, was reported by Inoue et.al.[56] to reduce CO_2 under UV illuminated into formate and methanol. After 7 h of illumination, more than 5 mM of methanol was produced in a 100 mL of purified water. The formate yield was reported ca. 1 mM at the same condition. Wang et al. have successfully applied Si nanowires as photoelectrodes to reduce CO_2[57] or combined Si nanowire with follow on organic reactions to fix and capture CO_2 to produce complex organics such as ibuprofen.[58]

12.6 Titanium oxide photoelectrodes

Oxide photoelectrodes have been extensively studied for water oxidation and to a lesser extent for hydrogen formation, but fewer examples on this type of photoelectrode have been explored for CO_2 reduction. TiO_2, is a wide band gap (∼3.0 eV)

n-type semiconductor. It is very stable, and by far the most popular and common photocatalyst, in general. In 1979, pioneering work[56] by Inoue, Fujishima and Honda showed that powdered TiO_2 suspended in water under UV illumination is able to reduce CO_2 to formic acid, formaldehyde, methanol and methane. Yates et al. have extensively studied mechanisms of TiO_2-based photocatalysis.[59] The large band gap of this material necessitates blue to UV optical excitation making this material a poor solar energy convertor. The efficient utilisation of solar energy requires the use of materials with a small band gap so that a large part of the visible light spectrum can be absorbed. Unfortunately, many promising semiconductors, especially oxides, have a wide band gap, which results in an onset of the absorption below 400 nm. A red-shift of this onset to the visible range is achieved by either sensitizing the semiconductor (Gratzel cell) or engineering its band gap. Anpo and Takeuchi have used this latter approach to extend the photocatalytic application of TiO_2 into visible range.[60] This research illustrated the design and development of highly reactive titanium oxide photocatalysts operating under visible light irradiation. The photocatalytic reactivity of semiconducting TiO_2 powder was found to be dramatically enhanced by the loading of small amounts of Pt, which work to enhance the charge separation of the electrons and holes generated by light.[60]

Single crystal n-TiO_2 electrodes were utilized as photoelectrodes for conversion of CO_2 to formic acid and methanol under high pressure conditions. High Faradaic yields of formate were obtained in an alkaline electrolyte, which was explained by the facilitated formation of hydrogen carbonate intermediates. However, methanol was detected only in acidic solution. The highest Faradaic efficiency for CO_2 reduction was reported as 22.1% (mainly HCOOH) at -1.2 V and 8 atm. CO_2 pressure.[61] Modified TiO_2 electrodes have also been explored. Pt-modified carbon black$-TiO_2$ was employed and methanol was identified as the main product at the initial stage and isopropanol production dominates after 10 h. The carbon dioxide conversion process was conducted under a galvanostatic condition with 0.02 mA/cm^2 current density, 0.5 M KCl and 10 mM pyridine (pH of the solution is 4.5$-$4.8).[62] To justify the assumption that electrochemical reduction of CO_2 involves dissociative chemisorption in the presence of hydrogen, TiO_2 mixed with other conductive oxide electrodes were fabricated for electrochemical CO_2 conversion. A current efficiency of 24% CH_3OH and 2% HCOOH was obtained at -0.9 V vs SCE with $RuO_2 + TiO_2$ ($35 + 65$ mol percent) in 0.2 M Na_2SO_4 saturated with CO_2. A Tafel plot at pH $= 1.2$ suggested that the first electron transfer is the rate-limiting step in the CO_2 reduction in this environment.[63]

12.7 Other oxides photoelectrode: Cu_2O, $CuFeO_2$, etc

Semiconducting oxidized copper electrodes have been studied for CO_2 reduction and reported in some cases to produce Faradaic efficiencies higher than 100% with onset potential as low as -0.4 V vs SCE for the conversion CO_2 into methanol.

A relative mechanism was proposed involving an absorption species of HCO_{ad}, from which three consecutive hydrogenations followed to form CH_3OH.[64] In all likelihood these electrodes are not stable and the apparent high Faradaic efficiencies are a misinterpretation of electrode photodecomposition processes.

An electrodeposited cuprous oxide thin film electrode was prepared and its reaction ability towards CO_2 reduction was compared with air-oxidized and anodized Cu electrodes. Methanol yield (38% Faradaic efficiencies) from the Cu_2O thin film electrode was found to be one order of magnitude higher than the anodized electrode and two orders of magnitude higher than the air-oxidized electrode. Surface analysis results indicated that the methanol yield was directly related to Cu(I) concentration on the surface. This result suggested a critical role of Cu(I) in the selective formation of CH_3OH, but copper oxides were found to be reduced to metallic Cu simultaneously in the CO_2 reduction process which introduces an ambiguity given the known catalytic activity of metallic copper.[21] An electrode fabricated from an air annealed Cu foil followed by electrochemical reduction to form a nano-wired Cu_2O layer was found to reduce CO_2 to CO and HCO_2H.[22] A Cu_2O layer formed at higher temperature (500 °C) produced a pronounced effect, including larger surface area and 0.5 V less overpotential than surfaces formed at lower temperature (130 °C). The activity of the modified electrode was stable for several hours under the reduction conditions and produced C_2 hydrocarbons at high overpotentials.

Recently, p-$CuFeO_2$ as a novel p-type semiconductor electrode containing a Cu(I) oxide was reported by Bocarsly and Cava to be active for CO_2 reduction.[65] The electrode was prepared by traditional solid state methods and the conductivity was controlled by Mg dopant concentration. The photoelectrode was found to be capable of reducing CO_2 to formate at 400 mV underpotential. The electrode material was found to undergo a very slow decomposition process during illumination. Still the electrode was found capable of operation for periods of the order of 10 h. This material was therefore much more stable than simple Cu_2O based photocathodes, suggesting that further design of complex oxides could produce systems showing good Faradaic yields for CO_2 reduction, along with long term stability.

12.8 Semiconductor with a molecular co-catalyst

Molecular catalysis of CO_2 reduction is arguably the most active research area among all electro- and photoelectrocatalytic systems. The concept of combining a molecular co-catalyst with a semiconductor dates back to 1980s when Bockris et al.[37,66–68] studied adsorbed species on silicon and p-CdTe photoelectrodes. Photoelectrochemical reduction of CO_2 by a diamond-coated Si electrodes has also been characterized by Ono et al.[69] Sato has reported an use of a visible-light-induced $[Ru(bpy)_2(CO)_2]$ electrocatalyst complex to selectively reduce CO_2 to formate on a p-type nitrogen-doped Ta_2O_5 semiconductor.[35,36] An interesting aspect of this

work is that the comparison between a ruthenium co-catalyst that is coordinated to the electrode surface, versus one that is present in solution. In this study a dramatic difference on the formate formation was noted with more than 10 times the quantity of product formed at the coordinated surface in comparison to the uncoordinated catalyst. A p-type InP semiconductor surface yielded a similar result when modified with an electropolymerized ruthenium polypyridyl complex.[36]

Homogeneous molecular co-catalysts dispersed on the semiconductor photoelectrode were investigated in the early 1980s. In 1983, Zafrir et al. reported the photoelectrochemical reduction of carbon dioxide to formic acid, formaldehyde and methanol on p-type gallium arsenide in an aqueous V(II)−V(III) chloride redox system.[70] Petit et al. reported that the system of p-type GaP or p-type GaAs with a homogeneous Ni(cyclam) catalyst was an efficient system for selective photoelectroreduction of carbon dioxide to carbon monoxide.[71,72] Parkinson and Weaver studied photochemically, electrochemically and photoelectrochemically-driven enzymatic redox processes. Most interestingly, a formate dehydrogenase enzyme was reported to work with an illuminated p-type InP semiconductor electrode to produce formate from aqueous CO_2 at visible light irradiation with a maximum yield of 89%.[73,74] [Re(Bu-bpy)(-$CO)_3$X] complexes have been extensively investigated by Kubiak et al.[75] and have been used to photoreduce CO_2 to CO on a p-type silicon photoelectrode in which the photovoltage was reported to exceed 600 mV.

Bocarsly's group has studied aqueous pyridinium as a catalyst to reduce CO_2 to formate, formaldehyde and methanol.[24,25,76] An aqueous pyridinium catalyst was reported to selectively photoelectrocatalytically reduce CO_2 to methanol at a p-type GaP semiconductor electrode.[6] As illustrated in Table 12.3, 96% Faradaic yield of methanol production was obtained at a current density of 0.21 mA/cm^2 at −0.2 V vs SCE which is 320 mV underpotential relative to the CO_2 to methanol's thermodynamic redox potential. This system is the first example of a PEC that reduces CO_2 to methanol at a photoinduced underpotential. A quantum efficiency for methanol formation was calculated to 12% (at 365 nm) at this potential. A lower working potential, gave more selective reduction towards methanol. Similar chemistry has also been applied to an illuminated iron pyrite electrode in combination with dissolved pyridinium or imidazolium co-catalysts to reduce CO_2 to CO and formic acid (imidazolium: CO 2.4%, formic acid, 4.9%; pyridinium: formic acid 2.7%, CO 0%). No methanol formation was reported in this iron pyrite system.[77] The striking difference between gallium phosphide and iron pyrite towards aqueous pyridinium co-catalyst assisting CO_2 reduction has been noted but not yet theoretically explained.

12.9 Semiconductors decorated with metal electrocatalysts for CO_2 reduction

Though a semiconducting cathode can generate charge upon optical excitation and deliver that charge to the semiconductor−electrolyte interface, such devices may

Table 12.3 Optical Conversion of CO_2 to Methanol by an Aqueous Pyridinium Catalyst Working with a p-Type GaP Photoelectrode

E (V)[a]	Underpot.[a] (mV)	*j* (mA/cm^2)	Faradaic eff. CH_3OH ξ (%)	Quantum yield Φ_{e^-} (%)	Quantum eff. CH_3OH Φ_{MeOH} (%)	OCE η (%)
465 nm						
−0.70	–	1.1	56	(8.3)[b]	(4.6)[b]	(1.3)[b]
−0.60	–	1.0	51	(5.1)[b]	(2.6)[b]	(1.3)[b]
−0.50	20	0.46	78	3.4	2.6_5	1.0_5
−0.40	120	0.33	83	2.3	1.9	1.0_3
−0.30	220	0.27	90	1.6	1.3_5	0.84
365 nm						
−0.50	20	0.92	62	71	44	10.9
−0.40	120	0.48	89	38	34	8.9
−0.30	220	0.28	92	16	15	5.8
−0.25	270	0.21	96	12	$11._5$	4.6_5
−0.20	320	0.21	96	13	$12._5$	4.8

[a] All potentials referenced versus SCE. Underpotentials stated are versus the standard potential of −0.52 V for the reduction of CO_2 to methanol at pH 5.2.
[b] These values were obtained at an overpotential and thus external electrical power was also used.
Adapted with permission from Reference 6.

not necessarily be stable under the conditions of CO_2 reduction nor have optimal catalytic properties for electron transfer into solution. Metals (as thin films or particles) have been used to modify semiconductor surfaces in order to stabilize the cathode surface and to catalyse CO_2 reduction via specific stabilization of CO_2 reduction intermediates. For example, Kaneco et al. have examined CO_2 reduction on p-InP photoelectrodes with Au, Ag, Ni, and Pb nanoparticle deposits.[78] They found that for Au and Ag modified cathodes, yields of CO increased relative to the bare p-InP, while Ni produced hydrocarbons at low yield and Pb produced more formic acid at higher yields than the bare semiconductor. All the reactions required high overpotentials, however, and thus solar energy conversion to fuels did not occur. A p-Si electrode modified with copper nanoparticles showed formation of hydrocarbons typical of reductions on Cu in addition to the CO and HCOOH formed at the bare p-Si electrode. A shift of +0.45 V in onset potential for CO_2 reduction was observed for copper particles on p-Si, but not for a continuous copper deposit on p-Si.[79] Modification of p-Si with Cu, Au, or Ag particles all lead to similar positive shifts in photovoltage.[80]

Recently, attention has been placed upon the effects of metal nanostructures upon the light absorbing properties of semiconductors. Metal nanoparticles such as Ag deposited on GaAs have been shown to increase scattering of light within the solar

cell device, thereby increasing light absorption.[81] The small size of metal nanostructures can result in surface plasmon resonances which alter the electric field at the semiconductor interface and improve absorbance in the visible region in addition to improving electron transfer at the interface.[82] For example, the quantum efficiency of CO_2 reduction at TiO_2 electrodes were improved by two orders of magnitude upon depositing gold on the TiO_2 surface.[83] Additionally, new product distribution leading to formic acid and methanol formation in addition to methane formation were observed upon gold deposition.

Another way in which metals are used in photoelectrochemical carbon dioxide reduction is in the Solar Thermal Electrochemical Photo (STEP) process pioneered by Stuart Licht. In this method, CO_2 reduction is effected at metal electrodes such as nickel, titanium or carbon, and light energy is used to both drive a semiconductor for electron transfer as well as to heat the cell, thereby altering the reaction thermodynamics and decreasing the applied potential required for electron transfer.[81–83] Licht's STEP process can be considered a hybrid process that combines aspects of photoelectrochemistry, electrochemistry, and thermal chemistry. As such it provides new opportunities to control the electrochemical interface and access critical thermochemical parameters. Overall, metal modified semiconductor interfaces appear to offer added benefits in catalysis and interfacial control; two topics of critical value in the search for efficient CO_2 conversion chemistry.

12.10 Summary, conclusion and prospect

In this chapter, we have summarized the previous achievements and also discussed the current progress of photoelectrocatalytic reduction of CO_2. The core chemistry of metal electrocatalysis driven by solar powered photovoltaics has been conceptually achieved, offering one pragmatic approach to solar fuels from CO_2. However, the efficiency of the systems presented to date are modest, and it is expected that pure photoelectrochemical systems may provide further improvements in efficiency. Modern developments in the metal electrocatalysts have been summarized with the hope that improved understanding of metal electrocatalytic CO_2 reduction might be coupled with light-driven semiconductors. The history and recent development of semiconductor materials in the field of CO_2 reduction chemistry has also been reviewed. The parameterizing factors of solar efficiency and quantum yield in semiconductor systems have been discussed. Four distinctive types of mechanistic CO_2 reduction by semiconductor system were delineated. Direct CO_2 reduction by semiconductor materials, CO_2 reduction by co-catalyst coordinated to the semiconductor surface, or simply homogeneous dispersed co-catalyst, or metal electrocatalyst decorated CO_2 reduction have been discussed as methods to couple light adsorption with catalytic materials.

In order to advance photoelectrochemical CO_2 reduction for energy storage and CO_2 utilisation, the following challenges must be overcome: (1) Materials

expense : Efficient CO_2 reduction still relies significantly on the use of noble metal elements, or other expensive catalytic systems, for example, ionic liquid as electrocatalysts. (2) Full cell reactions: Semiconductor powder or pure homogeneous photomolecular catalysts typically use a sacrificial electron donor. Coupling of photocathodic and photoanodic reactions for a complete catalytic system is challenging and tends to dramatically reduce system conversion efficiency. (3) Energy efficiency: The current efficiency and turnover frequency lead to overpotentials for CO_2 reduction which are not efficient enough to store a significant fraction of the applied energy. (4) Absorption efficiency: A photosensitizer that both maximally overlaps the solar spectrum and is highly catalytic for CO_2 reduction remains to be identified. (5) Mechanistic paradigms: The mechanism of electrocatalysis at semiconductor interfaces is often unknown. Plausible electrocatalytic mechanisms at metal electrodes have been proposed by Saveant[84], Hori[10], Kanan[22,27,30] and Bocarsly[86] however, mechanistic understanding in semiconductor systems is just starting to be addressed.[85] (6) Intermediate identification: The multiproton and multielectron transfers needed to reduce CO_2 produce reaction intermediates that are not well identified at this point.

Development of a CO_2 reduction process that operates efficiently and stably at a rate commensurate with the solar flux will ultimately determine if photoelectrochemical CO_2 reduction will be a significant part of our energy future. Such a challenge leaves many opportunities for future CO_2 chemists to advance.

Acknowledgements

The authors acknowledge support of this research from the United States Office of Basic Energy Sciences, Department of Energy under grant DE-SC0002133.

References

1. *Earth system research laboratory global monitoring division*. http://www.esrl.noaa.gov/gmd/ccgg/trends/; 2013 website [accessed on 30.10.13].
2. Kumar B, Llorente M, Froehlich J, Dang T, Sathrum A, Kubiak CP. *Annu Rev Phys Chem* 2012;**63**:541.
3. Sumida K, Rogow DL, Mason JA, McDonald TM, Bloch ED, Herm ZR, et al. *Chem Rev* 2012;**112**:724.
4. Aresta M. *Carbon dioxide as chemical feedstock*. Wiley-VCH; 2010, ISBN 978-3-527-32475-0.
5. Darensbourg DJ. *Chem Rev* 2007;**107**:2388.
6. Barton EE, Rampulla DM, Bocarsly AB. *J Am Chem Soc* 2008;**130**:6342.
7. Sakakura T, Choi JC, Yasuda H. *Chem Rev* 2007;**107**:2365.
8. Appel AM, Bercaw JE, Bocarsly AB, Dobbek H, DuBois DL, Dupuis M, et al. *Chem Rev* 2013;**113**:6621.
9. Royer E. *C R Acad Sci* 1870;**70**:731.
10. Hori Y, Wakebe H, Tsukamoto T, Koga O. *Electrochimica Acta* 1994;**39**:1833.

11. Nosaka Y, Fox MA. *J Phys Chem* 1988;**92**:1893.
12. Tran PD, Nguyen M, Pramana SS, Bhattacharjee A, Chiam SY, Fize J, et al. *Energy & Environ Sci* 2012;**5**:8912.
13. Habisreutinger SN, Schmidt-Mende L, Stolarczyk JK. *Angew Chem Int Ed* 2013;**52**: 7372.
14. Nozik AJ. *Annu Rev Phys Chem* 1978;**29**:189.
15. Walter MG, Warren EL, McKone JR, Boettcher SW, Mi QX, Santori EA, et al. *Chem Rev* 2010;**110**:6446.
16. Kuhl KP, Cave ER, Abram DN, Jaramillo TF. *Energy & Environ Sci* 2012;**5**:7050.
17. Angamuthu R, Byers P, Lutz M, Spek AL, Bouwman E. *Science* 2010;**327**:313.
18. Peterson AA, Abild-Pedersen F, Studt F, Rossmeisl J, Norskov JK. *Energy & Environ Sci* 2010;**3**:1311.
19. Yang NJ, Gao F, Nebel CE. *Anal Chem* 2013;**85**:5764.
20. Xu ZC, Lai EC, Yang SH, Hamad-Schifferli K. *Chem Commun* 2012;**48**:5626.
21. Le M, Ren M, Zhang Z, Sprunger PT, Kurtz RL, Flake JC. *J Electrochem Soc* 2011;**158**: E45.
22. Li CW, Kanan MW. *J Am Chem Soc* 2012;**134**:7231.
23. Rosen BA, Salehi-Khojin A, Thorson MR, Zhu W, Whipple DT, Kenis PJA, et al. *Science* 2011;**334**:643.
24. Yan YZ, E. L, Gu J, Bocarsly AB. *J Am Chem Soc* 2013;**135**:14020.
25. Cole EB, Lakkaraju PS, Rampulla DM, Morris AJ, Abelev E, Bocarsly AB. *J Am Chem Soc* 2010;**132**:11539.
26. DiMeglio JL, Rosenthal J. *J Am Chem Soc* 2013;**135**:8798.
27. Chen YH, Kanan MW. *J Am Chem Soc* 2012;**134**:1986.
28 White JL, Herb JT, Kaczur JJ, Majsztrik PW, Bocarsly AB. Photons to formate: Efficient electrochemical solar energy conversion via reduction of carbon dioxide. *Journal of CO_2 Utilization* 2014;**7**:1−5.
29. Yotsuhashi S, Hashiba H, Deguchi M, Zenitani Y, Hinogami R, Yamada Y, Deura M, Ohkawa K. *Aip Adv* 2012;**2**:042160.
30. Chen YH, Li CW, Kanan MW. *J Am Chem Soc* 2012;**134**:19969.
31. Nie XW, Esopi MR, Janik MJ, Asthagiri A. *Angew Chem Int Ed* 2013;**52**:2459.
32. Taniguchi I, Aurianblajeni B, Bockris JO. *J Electroanal Chem* 1983;**157**:179.
33. Montoya JH, Peterson AA, Norskov JK. *Chemcatchem* 2013;**5**:737.
34. Halmann M. *Nature* 1978;**275**:115.
35. Sato S, Morikawa T, Saeki S, Kajino T, Motohiro T. *Angew Chem Int Ed* 2010;**49**:5101.
36. Arai T, Sato S, Uemura K, Morikawa T, Kajino T, Motohiro T. *Chem Commun* 2010;**46**: 6944.
37. Bockris JO, Wass JC. *J Electrochem Soc* 1989;**136**:2521.
38. Inoue T, Fujishima A, Konishi S, Honda K. *Nature* 1979;**277**:637.
39. Aurian-Blajeni B, Halmann M, Manassen J. *Sol Energy Mater* 1983;**8**:425.
40. Flaisher H, Tenne R, Halmann M. *J Electroanal Chem* 1996;**402**:97.
41. Kaneco S, Katsumata H, Suzuki T, Ohta K. *Chem Eng J* 2006;**116**:227.
42. Hirota K, Tryk DA, Hashimoto K, Okawa M, Fujishima A. *J Electrochem Soc* 1998;**145**: L82.
43. Hirota K, Tryk DA, Yamamoto T, Hashimoto K, Okawa M, Fujishima A. *J Phys Chem B* 1998;**102**:9834.
44. Zafrir M, Ulman M, Zuckerman Y, Halmann M. *J Electroanal Chem Interfacial Electrochem* 1983;**159**:373.

45. Yotsuhashi S, Deguchi M, Hashiba H, Zenitani Y, Hinogami R, Yamada Y, et al. *Appl Phys Lett* 2012;**100**:243904.
46. Yotsuhashi S, Deguchi M, Zenitani Y, Hinogami R, Hashiba H, Yamada Y, et al. *Appl Phys Express* 2011;**4**:7101.
47. Taniguchi I, Aurian-Blajeni B, Bockris JOM. *J Electroanal Chem Interfacial Electrochem* 1983;**157**:179.
48. Aurian-Blajeni B, Ahsan Habib M, Taniguchi I, Bockris JOM. *J Electroanal Chem Interfacial Electrochem* 1983;**157**:399.
49. Taniguchi I, Aurian-Blajeni B, Bockris JOM. *Electrochim Acta* 1984;**29**:923.
50. Yoneyama H, Sugimura K, Kuwabata S. *J Electroanal Chem Interfacial Electrochem* 1988;**249**:143.
51. Taniguchi I, Aurian-Blajeni B, Bockris JOM. *J Electroanal Chem Interfacial Electrochem* 1984;**161**:385.
52. Chandrasekaran K, Bockris JO. *Electrochim Acta* 1987;**32**:1393.
53. Bockris JOM, Wass JC. *J Electrochem Soc* 1989;**136**:2521.
54. Liu R, Stephani C, Tan K, Wang D. *Angew Chem Int Ed* 2013;**52**:4225.
55. Liu R, Yuan G, Joe C, Lightburn T, Tan K, Wang D. *Angew Chem Int Ed* 2012;**51**:6709.
56. Anpo M, Takeuchi M. *J Catal* 2003;**216**:505.
57. Halmann M, Aurian-Blajeni B. *J Electroanal Chem* 1994;**375**:379.
58. de Tacconi NR, Chanmanee W, Dennis BH, MacDonnell FM, Boston DJ, Rajeshwar K. *Electrochem Solid-state Lett* 2011;**15**:B5.
59. Linsebigler AL, Lu GQ, Yates JT. *Chem Rev* 1995;**95**:735.
60. Bandi A. *J Electrochem Soc* 1990;**137**:2157.
61. Frese KW. *J Electrochem Soc* 1991;**138**:3338.
62. Yano J, Morita T, Shimano K, Nagami Y, Yamasaki S. *J Solid State Electrochem* 2007;**11**:554.
63. Gu J, Wuttig A, Krizan JW, Hu Y, Detweiler ZM, Cava RJ, et al. *J Phys Chem C* 2013;**117**:12415.
64. Aurianblajeni B, Taniguchi I, Bockris JO. *J Electroanal Chem* 1983;**149**:291.
65. Aurianblajeni B, Habib MA, Taniguchi I, Bockris JO. *J Electroanal Chem* 1983;**157**:399.
66. Ono H, Yokosuka A, Tasiro T, Morisaki H, Yugo S. *New Diam Front Carbon Technol* 2002;**12**:141.
67. Zafrir M, Ulman M, Zuckerman Y, Halmann M. *J Electroanal Chem* 1983;**159**:373.
68. Petit JP, Chartier P, Beley M, Sauvage JP. *New J Chem* 1987;**11**:751.
69. Petit JP, Chartier P, Beley M, Deville JP. *J Electroanal Chem* 1989;**269**:267.
70. Parkinson BA, Weaver PF. *Nature* 1984;**309**:148.
71. Parkinson BA, Weaver PF. *J Electrochem Soc* 1984;**131**:C324.
72. Kumar B, Smieja JM, Kubiak CP. *J Phys Chem C* 2010;**114**:14220.
73. Yan YGJ, Bocarsly AB. *Aerosol Air Qual Res* 2014;**14**:515.
74. Bocarsly AB, Gibson QD, Morris AJ, L'Esperance RP, Detweiler ZM, Lakkaraju PS, et al. *ACS Catal* 2012;**2**:1684.
75. Kaneco S, Katsumata H, Suzuki T, Ohta K. *Appl Catal B: Environ* 2006;**64**:139.
76. Hinogami R, Mori T, Yae S, Nakato Y. *Chem Lett* 1994;**23**:1725.
77. Hinogami R, Nakamura Y, Yae S, Nakato Y. *J Phys Chem B* 1998;**102**:974.
78. Nakayama K, Tanabe K, Atwater HA. *Appl Phys Lett* 2008;**93**:121904.
79. Schaadt DM, Feng B, Yu ET. *Appl Phys Lett* 2005;**86**:063106.
80. Hou W, Hung WH, Pavaskar P, Goeppert A, Aykol M, Cronin SB. *ACS Catal* 2011;**1**:929.

81. Licht S. *J Phys Chem C* 2009;**113**:16283.
82. Licht S, Wang B, Ghosh S, Ayub H, Jiang D, Ganley J. *J Phys Chem Lett* 2010;**1**:2363.
83. Licht S, Wang B, Wu H. *J Phys Chem C* 2011;**115**:11803.
84. Amatore C, Pinson J, Saveant JM, Thiebault A. *J Am Chem Soc* 1981;**103**:6930.
85. Munoz-Garcia AB, Carter EA. *J Am Chem Soc* 2012;**134**:13600.
86 Detweiler ZM, White JL, Bernasek SL, Bocarsly AB. Anodized Indium Metal Electrodes for Enhanced Carbon Dioxide Reduction in Aqueous Electrolyte. *Langmuir*; 2014.
87 Komatsu S, Yanagihara T, Hiraga Y, Tanaka M, Kunugi A. *Denki Kagaku* 1995;**63**:217.